ISSN 1674-1056
http://cpb.iphy.ac.cn
http://iopscience.iop.org/cpb
中国物理 B
Chinese Physics
中国物理 Chinese Physics B

Effects of oxygen vacancy concentration and temperature on memristive behavior of $SrRuO_3$/Nb:$SrTiO_3$junctions

Zhi-Cheng Wang(王志成), Zhang-Zhang Cui(崔璋璋), Hui Xu(徐珲), Xiao-Fang Zhai(翟晓芳), Ya-Lin Lu(陆亚林)
Citation: Chin. Phys. B . 2019, 28(8): 087303 . **doi:** 10.1088/1674-1056/28/8/087303
Journal homepage: http://cpb.iphy.ac.cn; http://iopscience.iop.org/cpb

What follows is a list of articles you may be interested in

Electronic synapses based on ultrathin quasi-two-dimensional gallium oxide memristor

Shuopei Wang(王硕培), Congli He(何聪丽), Jian Tang(汤建), Rong Yang(杨蓉), Dongxia Shi(时东霞), Guangyu Zhang(张广宇)
Chin. Phys. B . 2019, 28(1): 017304 . **doi:** 10.1088/1674-1056/28/1/017304

Coexistence of unipolar and bipolar modes in Ag/ZnO/Pt resistive switching memory with oxygen-vacancy and metal-Ag filaments

Han-Lu Ma(马寒露), Zhong-Qiang Wang(王中强), Hai-Yang Xu(徐海阳), Lei Zhang(张磊), Xiao-Ning Zhao(赵晓宁), Man-Shu Han(韩曼舒), Jian-Gang Ma(马剑钢), Yi-Chun Liu(刘益春)
Chin. Phys. B . 2016, 25(12): 127303 . **doi:** 10.1088/1674-1056/25/12/127303

Bipolar resistance switching in the fully transparent $BaSnO_3$-based memory device

Zhang Ting, Yin Jiang, Zhao Gao-Feng, Zhang Wei-Feng, Xia Yi-Dong, Liu Zhi-Guo
Chin. Phys. B . 2014, 23(8): 087304 . **doi:** 10.1088/1674-1056/23/8/087304

Oxygen vacancy in N-doped Cu_2O crystals: A density functional theory study

Li Min, Zhang Jun-Ying, Zhang Yue, Wang Tian-min
Chin. Phys. B . 2012, 21(8): 087301 . **doi:** 10.1088/1674-1056/21/8/087301

The influence of interfacial barrier engineering on the resistance switching of In_2O_3:SnO_2/TiO_2/In_2O_3:SnO_2 device

Liu Zi-Yu,Zhang Pei-Jian,Meng Yang,Li Dong,Meng Qing-Yu,Li Jian-Qi,Zhao Hong-Wu
Chin. Phys. B . 2012, 21(4): 047302 . **doi:** 10.1088/1674-1056/21/4/047302

Effects of oxygen vacancy concentration and temperature on memristive behavior of $SrRuO_3$/Nb:$SrTiO_3$ junctions*

Zhi-Cheng Wang(王志成)[1], Zhang-Zhang Cui(崔璋璋)[2,3,†], Hui Xu(徐珲)[1], Xiao-Fang Zhai(翟晓芳)[1,3], and Ya-Lin Lu(陆亚林)[1,2,3,‡]

[1] *Hefei National Laboratory for Physical Sciences at Microscale, University of Science and Technology of China, Hefei* 230026, *China*
[2] *National Synchrotron Radiation Laboratory, University of Science and Technology of China, Hefei* 230026, *China*
[3] *Synergy Innovation Center of Quantum Information and Quantum Physics, University of Science and Technology of China, Hefei* 230026, *China*

(Received 9 April 2019; revised manuscript received 6 June 2019; published online 25 July 2019)

Metal/semiconductor memristive heterostructures have potential applications in nonvolatile memory and computing devices. To enhance the performance of the memristive devices, it requires a comprehensive engineering to the metal/semiconductor interfaces. Here in this paper, we discuss the effects of oxygen vacancies and temperature on the memristive behaviors of perovskite-oxide Schottky junctions, each consisting of $SrRuO_3$ thin films epitaxially grown on Nb:$SrTiO_3$ substrates. The oxygen partial pressure and laser fluence are controlled during the film growth to tune the oxygen defects in $SrRuO_3$ films, and the Schottky barrier height can be controlled by both the temperature and oxygen vacancies. The resistive switching measurements demonstrate that the largest resistance switching ratio can be obtained by controlling oxygen vacancy concentration at lower temperature. It suggests that reducing Schottky barrier height can enhance the resistive switching performance of the $SrRuO_3$/Nb:$SrTiO_3$ heterostructures. This work can conduce to the development of high-performance metal-oxide/semiconductor memristive devices.

Keywords: memristor, oxygen vacancy, Schottky barrier

PACS: 73.63.–b, 81.07.–b, 73.22.–f , 68.55.Ln **DOI:** 10.1088/1674-1056/28/8/087303

1. Introduction

In recent years, the memristive switching devices have received intensive attention for the applications in the resistive random access memories (RRAM) because of their many superiorities such as the simple structure, outstanding performance, low power consumption, and fast switching.[1] The memory effect has been achieved by the switching between the high resistance state (HRS, OFF state) and the low resistance state (LRS, ON state), modulated by the electrically unipolar or bipolar bias. Great efforts have been made to discover the microscopic origins of resistive switching, which is important for understanding this physical phenomenon and is the key point for further enhancing the resistive switching performance. A variety of resistive switching devices have been fabricated while the mechanisms responsible for the memristive behaviors are heavily disputed. It can be concluded that the possible mechanisms include ion migration and thermochemical reaction, metal-insulator transition, charge trapping or detraping, *etc*.[2–6] These findings highlight the way such as ion doping and defect engineering to enhance the memristive performance, in which the oxygen vacancies are extensively studied because of the ideal investigating platform provided by the transition-metal oxides.

Both of the binary and complex transition-metal perovskite oxides are widely used in the resistive switching devices due to the stable crystal structures and rich electronic properties.[7–16] Among them, $SrRuO_3$ (SRO) is a ferromagnetic metal with a high work function and Nb:$SrTiO_3$ (Nb:STO) is an n-type semiconductor.[17] The resistive switching behavior of SRO/Nb:STO heterostructures has been studied previously,[6] in which the Nb content was controlled and it was demonstrated that the dependence of electron charging in a self-trap on bias polarity leads to the resistive switching behavior, but how the oxygen vacancy concentration affects the resistive switching behavior has not been revealed. And the modulation of the Schottky barrier height to the memristive performance, which may determine the resistive switching behavior fundamentally, is still unclear.

In this work, we systematically study the effects of oxygen vacancy concentration and Schottky barrier height on the resistive switching behavior of SRO/Nb:STO heterostructures prepared by pulsed laser deposition (PLD) technique assisted with reflective high-energy electron diffraction (RHEED). During the film growth, we control the oxygen partial pressure and laser fluence to tune the oxygen vacancy concentration in the SRO film. Besides, the Schottky barrier height can be modulated by both the oxygen vacancy concentration and the temperature. The resistance switching measure-

*Project supported by the National Natural Science Foundation of China (Grant Nos. 51627901 and 11574287), the National Key Research and Development Program of China (Grant No. 2016YFA0401004), and the Anhui Initiative in Quantum Information Technologies, China (Grant No. AHY100000).

†Corresponding author. E-mail: zzcui@ustc.edu.cn
‡Corresponding author. E-mail: yllu@ustc.edu.cn

© 2019 Chinese Physical Society and IOP Publishing Ltd

ments of SRO/Nb:STO heterostructures demonstrate that all the films exhibit resistive switching behaviors that depend strongly on the concentration of oxygen vacancies and the temperature, and the heterostructures exhibit the best memristive performance at a smaller Schottky barrier height. These findings may be instructive to the future development of resistive switching devices with high performance.

2. Experiments

The $SrRuO_3$ thin films, each with a thickness of ~ 10 nm, were grown on (001)-oriented Nb:$SrTiO_3$ single-crystal substrates with Nb doping of 0.7 wt% by the PLD. A KrF excimer laser beam ($\lambda = 248$ nm) was focused onto the SRO target at a repetition rate of 1 Hz, and the laser fluence was 1 J/cm^2 and 1.5 J/cm^2 separately. The substrate temperature was ~ 700 °C in the whole deposition process. The oxygen pressures in the growth chamber were 0.1 Pa, 5 Pa, and 15 Pa respectively. After being deposited, the films were cooled down to room temperature under an oxygen pressure of 100 Pa. The x-ray diffraction (XRD) analysis was performed by using a Rigaku 4-circle diffractometer with a Cu Kα anode radiation (wavelength of 1.5406 Å) to investigate the structural quality and lattice constants of SRO films. The temperature-dependent current–voltage (I–V) characteristics in a range from 300 K to 20 K were measured by a quantum design physical property measurement system (PPMS) and a Keithley 2400 Source Meter, in which the DC voltage was applied to the samples and the electric currents were measured. The films and substrates were connected by gold wires and silver paste. The Ru M-edge and O K-edge soft x-ray absorption spectrum (XAS) measurements were performed at beamline BL12B-a at the National Synchrotron Radiation Laboratory of China (NSRL).

3. Results and discussion

During the film growth, the ambient oxygen partial pressure and the laser fluence are varied to control the oxygen vacancy density in SRO films. Three groups of SRO thin films are grown under oxygen partial pressures of 0.1 Pa, 5 Pa, and 15 Pa with a laser fluence of 1 J/cm^2 respectively and one group of SRO thin films were grown at 5 Pa with a laser fluence of 1.5 J/cm^2. Figure 1(a) shows the XRD ω–2θ scans around the Nb:STO (001) and (002) Bragg reflections of the SRO films. All the samples are aligned well on the XRD instrument platform, the acquired patterns have strong comparability. As figure 1(a) shows, all the thin films exhibit the expected a (001)-oriented structure. The out-of-plane lattice constant c values of the SRO films are obtained from the positions of (001) and (002) Bragg reflections and the results are summarized in Fig. 1(b), where the red point represents the c value of SRO film grown at 5 Pa with a laser fluence of 1.5 J/cm^2. We consider $\pm 0.02°$ (the step we used during the XRD test) as the error, and the peak positions are indeed within this range. As can be seen, the c value decreases with oxygen partial pressure and laser fluence increasing. This is consistent with previous reports on SRO films, and the reason is ascribed to the variation of oxygen vacancies under different growth conditions that the perovskite-oxide lattice will expand when there are more oxygen vacancies.[18,19]

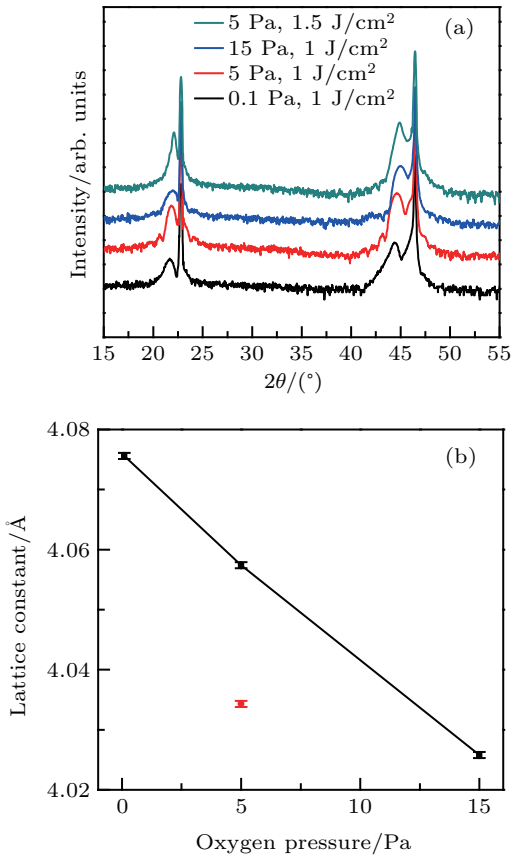


Fig. 1. (a) XRD ω–2θ scans of SRO/Nb:STO heterostructures, and (b) out-of-plane lattice constants of SRO films calculated from the XRD SRO (001) and (002) peaks. The red point represents the SRO film grown at 5 Pa and 1.5 J/cm^2.

Figure 2 shows the I–V characteristics of the SRO/Nb:STO samples measured in a temperature range from 300 K to 20 K. The positive bias is defined as the electric current flowing from the Nb:STO substrate to the SRO layer (see the device geometry in Fig. 2(a)). The electric currents are measured at each temperature, following a voltage sweep from 0 V $\rightarrow -5$ V $\rightarrow 0$ V $\rightarrow 5$ V $\rightarrow 0$ V. As seen in Figs. 2(b)–2(e), the I–V characteristics of all the heterostructures especially for the SRO films grown at 5 Pa and 15 Pa, clearly show a rectifying effect that arises from the Schottky barrier between the SRO film and Nb:STO substrate. In the forward bias (negative voltage), upon increasing the voltage, the width of the depletion region and the built-in electric field in Nb:STO decrease. While in the reverse bias (positive voltage), upon increasing the voltage, the width of the depletion region and the built-in electric field increase. Furthermore, each of the I–V curves of

all the samples in the reverse bias region shows a clear hysteretic response to the resistance, which is the evidence of the colossal electroresistance (CER) effect. The heterostructures can be electrically switched between the low resistance state (with voltage sweeping from 0 V to 5 V) and the high resistance state (with voltage sweeping from 5 V to 0 V).

Figure 2(f) summarizes the resistance ratios of HRS to LRS (R_{OFF}/R_{ON} or I_{LRS}/I_{HRS}) at 20 K of the SRO/Nb:STO heterostructures under different conditions. It can be seen that the *I*–*V* characteristics of the four samples are very different. For the films grown at 5 Pa and 15 Pa, the largest resistance ratio of HRS to LRS (I_{LRS}/I_{HRS}) at the same bias voltage range between 0 V and 5 V increases significantly with temperature decreasing. At the lowest measuring temperature of 20 K, I_{LRS}/I_{HRS} of the film grown at 5 Pa and 1 J/cm^2 reaches to the largest value of ~ 10 at ~ 2.4 V. While for the SRO films grown at 0.1 Pa and 15 Pa, the largest I_{LRS}/I_{HRS} values decrease to about 1.3 and 2.1, respectively. Besides, the *I*–*V* curves of the SRO films grown at 0.1 Pa are twisted, which indicates that the excessive oxygen vacancies may disturb the resistive switching behavior. This phenomenon is probably caused by the degenerated interfacial epitaxial quality and microstructural disorders in SRO films at such a low oxygen pressure.[20,21] Furthermore, as the laser fluence increases from 1 J/cm^2 to 1.5 J/cm^2, a similar effect is observed that the largest I_{LRS}/I_{HRS} values of SRO films grown at 5 Pa and 1.5 J/cm^2 are about 2.4. These results indicate that the appropriate control of oxygen vacancy concentration is important for enhancing the resistive switching performance of SRO/Nb:STO heterostructures. It should be noted that we prepare a series of samples under different fabrication condition and perform repeated measurements on each sample, and the results are highly repeatable.

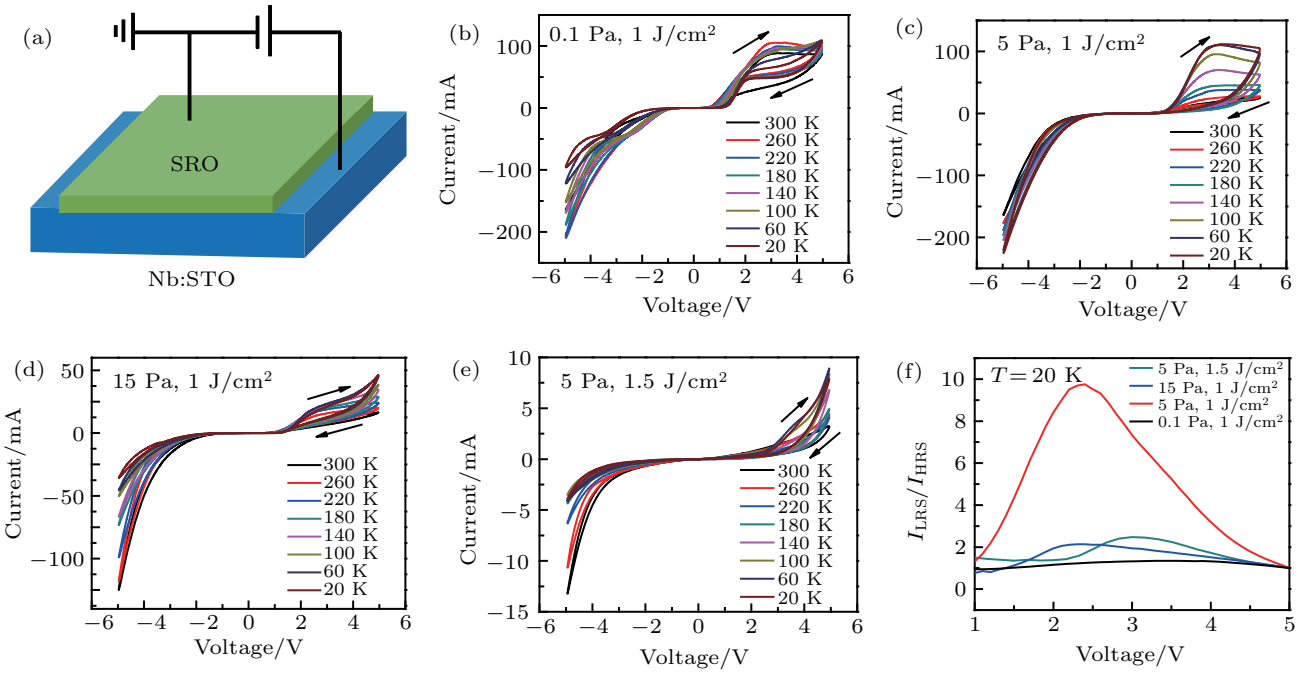


Fig. 2. (a) Device geometry of SRO/Nb:STO heterostructure. A DC voltage is applied across the film and substrate. (b)–(e) Temperature-dependent current (*I*)–volatge (*V*) characteristics of the SRO/Nb:STO heterostructures measured at temperatures ranging from 300 K to 20 K. Up arrow and down arrow indicate voltage sweep direction. (f) Ratios of HRS current to LRS current (I_{LRS}/I_{HRS}) at 20 K calculated from panels (b)–(e).

To verify the change of oxygen vacancy concentration in the SRO films prepared at different oxygen pressures and laser fluence, we perform the Ru *M*-edge and O *K*-edge x-ray absorption spectrum measurement. Figure 3(a) shows the Ru *M*-edge x-ray absorption spectra. The two main peaks at 460 eV (indicated by dashed line) and 482 eV originate from the transitions from spin–orbit splitted Ru $3p_{3/2}$ and $3p_{1/2}$ to the Ru 4d.[22] The spectral profiles of the SRO films are very similar and the peak positions do not show notable shift, indicating that the valence states of Ru ions do not change in these samples. Figure 3(b) shows the O *K*-edge x-ray absorption spectra of the SRO films. The absorption peaks around 529 eV (indicated by dashed line) are due to the transitions from O 1s to the hybridized state of O 2p and Ru 4d t_{2g} orbitals, and the group of peaks in a range from 531 eV to 544 eV are due to the transitions to Ru 4d e_g, Sr 4d, and Ru 5sp states.[23–26] Though the peak positions of Ru 4d t_{2g} states of different SRO films have no distinguishable change, it can be clearly seen that the intensity of this peak increases with oxygen partial pressure and laser fluence increasing (see Fig. 3(c)). It is well known that the x-ray absorption spectrum peak intensity is closely related to the density of unoccupied states.[27] The decrease of oxygen vacancy concentration in the SRO film can increase the density of electron holes in the O 2p and Ru 4d hybridized state,

leading to higher intensity of the Ru 4d t_{2g} absorption peak. It should be noted that though the valance of Ru does not change, the Sr 4d absorption peak shifts monotonically to lower energy with oxygen vacancy concentration decreasing. It has been reported previously that the valence of Ru is more stable than that of Sr in different chemical environment.[28] So it is possible that the Sr valence changes while the Ru valence remains unchanged in the SRO films with different oxygen vacancy concentrations. Thus, the O *K*-edge x-ray absorption spectrum gives the clear evidence that the concentration of oxygen vacancies in the SRO film decreases with the increase of oxygen pressure and laser fluence, which is consistent with the x-ray diffraction result. It indicates that the distinct memristive characteristics of the SRO/Nb:STO heterostructures at the same temperature are due to the change of the oxygen vacancies in the SRO films.

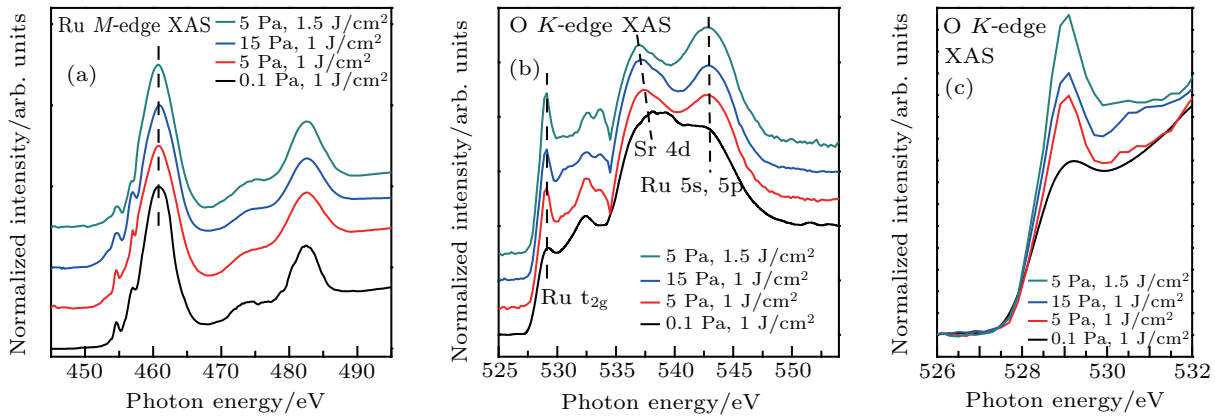


Fig. 3. (a) Ru *M*-edge and (b) O *K*-edge XAS spectra of SRO films. (c) Magnified Ru 4d t_{2g} absorption peaks in the O *K*-edge XAS spectra of SRO films. All the XAS spectra are normalized to the incoming photon flux and the post-edge intensity.

To check whether the Schottky barrier height (illustrated in Fig. 4(a)) of the SRO/Nb:STO heterostructures is changed by oxygen vacancy and temperature, the standard semiconductor Schottky barrier model is used to calculate the Schottky barrier height.[17,18] This model is expressed as the following relationship between I and V under forward bias (negative voltage)

$$I = A^* S T^2 \exp\left(-\frac{q\Phi_B}{k_B T}\right) \exp\left(\frac{qV}{nk_B T}\right). \quad (1)$$

Here, q is the electron charge, k_B is the Boltzmann's constant, V is the applied bias, T is the temperature, S is the junction area, A^* is the Richardson's constant, Φ_B is the Schottky barrier height at zero bias, and n is an ideality factor. According to Eq. (1), the Φ_B value can be obtained by fitting the I–V curves through using the thermionic emission theory. Figure 4(b) shows the fitting of I–V curves measured at 20 K under forward bias. In the low V region prior to the saturation of I because of series resistance such as electrode/SRO and electrode/Nb:STO resistance, the log$I$–V characteristics fit well with the straight lines. It can be clearly seen that the intersection of I at $V = 0$ is the largest for the sample grown at 5 Pa and 1 J/cm^2, which means the smallest Φ_B value. The derived Φ_B values from 300 K to 20 K are illustrated in Fig. 4(c). As can be seen, the Schottky barrier height can be changed by both the oxygen vacancies and the temperature. At temperatures below 140 K, the Φ_B values of the SRO/Nb:STO grown at 5 Pa and 1 J/cm^2 are the smallest, accompanied by the notable enhancement of memristive performance of this sample. Besides, for each sample, Φ_B decreases significantly with temperature lowing. We show that for the SRO films grown at 5 Pa and 15 Pa, the memristive performances are significantly improved at lower temperatures. This can be attributed to the reduced Schottky barrier height of the SRO/Nb:STO junction.

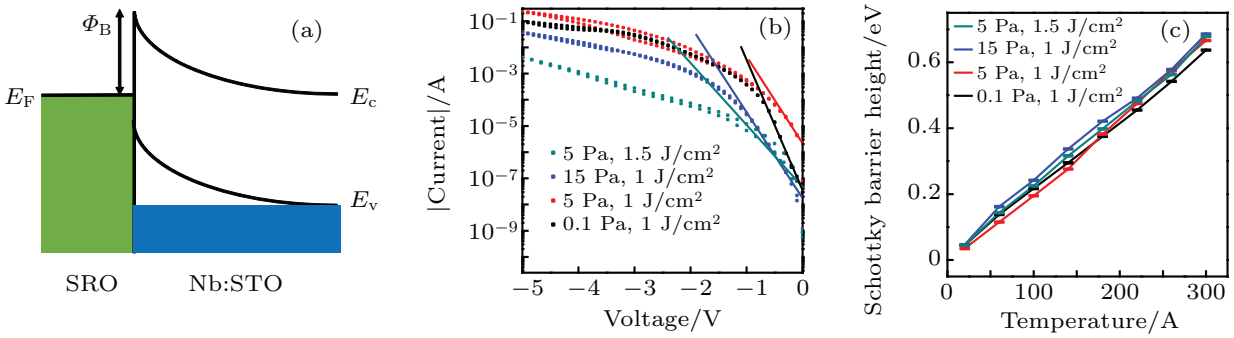


Fig. 4. (a) Sketch of Schottky barrier height of SRO/Nb:STO system. (b) Fitting of $|I|$–V data measured at 20 K to thermionic emission equation for SRO/Nb:STO heterostructures. (c) Temperature dependence of Schottky barrier heights of the SRO/Nb:STO heterostructures.

4. Conclusions

In this work, we systematically study the effects of the oxygen vacancy concentration and Schottky barrier height on the resistive switching behavior of SRO/Nb:STO heterostructures. The XRD and XAS measurements demonstrate that the oxygen vacancy concentrations in the SRO films are reduced by increasing the growth oxygen partial pressure and laser fluence. The fitting of the rectifying *I*–*V* characteristics of the films by using the thermionic emission theory shows that the Schottky barrier height decreases with temperature lowering. The temperature dependent resistive switching measurements demonstrate the performance of the SRO/Nb:STO junctions can be enhanced by modulating the oxygen vacancy concentration and temperature. The resistive switching behavior of the SRO/Nb:STO junctions can be driven by the migration of oxygen ions or the charging effect at the Schottky interface. Both mechanisms are closely related to the oxygen vacancy concentration and Schottky barrier height. Our results could be instructive to future develop the high-performance resistive switching metal-oxide/semiconductor devices.

References

[1] Janousch M, Meijer G I, Staub U, Delley B, Karg S F and Andreasson B P 2007 *Adv. Mater.* **19** 2232

[2] Shibuya K, Dittmann R, Mi S and Waser R 2010 *Adv. Mater.* **22** 411

[3] Lee M J, Lee C B, Lee D, Lee S R, Chang M, Hur J H, Kim Y B, Kim C J, Seo D H and Seo S 2011 *Nat. Mater.* **10** 625

[4] Wu D, Jiang Y, Yu Y, Zhang Y, Li G, Zhu Z, Wu C, Wang L, Luo L and Jie J 2012 *Nanotechnology* **23** 485203

[5] Pan F, Gao S, Chen C, Song C and Zeng F 2014 *Mater. Sci. Eng. R* **83** 1

[6] Fujii T, Kawasaki M, Sawa A, Kawazoe Y, Akoh H and Tokura Y 2007 *Phys. Rev. B* **75** 165101

[7] Waser R, Dittmann R, Staikov G and Szot K 2009 *Adv. Mater.* **21** 2632

[8] Jiang A Q, Wang C, Jin K J, Liu X B, Scott J F, Hwang C S, Tang T A, Lu H B and Yang G Z 2011 *Adv. Mater.* **23** 1277

[9] Lee E, Gwon M, Kim D W and Kim H 2011 *Appl. Phys. Lett.* **98** 132905

[10] Lee H S, Choi S G, Park H H and Rozenberg M 2013 *Sci. Rep.* **3** 1704

[11] Xu N, Liu L, Sun X, Liu X, Han D, Wang Y, Han R, Kang J and Yu B 2008 *Appl. Phys. Lett.* **92** 232112

[12] Chang W Y, Liao J H, Lo Y S and Wu T B 2009 *Appl. Phys. Lett.* **94** 172107

[13] Do Y H, Kwak J S, Bae Y C, Jung K, Im H and Hong J P 2009 *Appl. Phys. Lett.* **95** 093507

[14] Goux L, Lisoni J, Jurczak M, Wouters D, Courtade L and Muller C 2010 *J. Appl. Phys.* **107** 024512

[15] Yan Z, Guo Y, Zhang G and Liu J M 2011 *Adv. Mater.* **23** 1351

[16] Deng X L, Hong S, Hwang I, Kim J S, Jeon J H, Park Y C, Lee J, Kang S O, Kawai T and Park B H 2012 *Nanoscale* **4** 2029

[17] Rana K G, Khikhlovskyi V and Banerjee T 2012 *Appl. Phys. Lett.* **100** 213502

[18] Maria J, Trolier-McKinstry S, Schlom D, Hawley M and Brown G 1998 *J. Appl. Phys.* **83** 4373

[19] Kamo T, Nishida K, Akiyama K, Sakai J, Katoda T and Funakubo H 2007 *Jpn. J. Appl. Phys.* **46** 6987

[20] Yoo Y Z, Chmaissem O, Kolesnik S, Dabrowski B, Maxwell M and Kimball C W 2005 *J. Appl. Phys.* **97** 103525

[21] Lu W L, He K H, Song W D, Sun C J, Chow G M and Chen J S 2013 *J. Appl. Phys.* **113** 17E125

[22] Harano T, Shibata G, Ishigami K, Takashashi Y, Verma V, Singh V, Kadono T, Fujimori A, Takeda Y and Okane T 2013 *Appl. Phys. Lett.* **102** 222404

[23] Noh H J, Oh S J, Park B G, Park J H, Kim J Y, Kim H D, Mizokawa T, Tjeng L H, Lin H J, Chen C T, Schuppler S, Nakatsuji S, Fukazawa H and Maeno Y 2005 *Phys. Rev. B* **72** 052411

[24] Abbate M, Guevara J A, Cuffini S L, Mascarenhas Y P and Morikawa E 2002 *Eur. Phys. J. B* **25** 203

[25] Cui Z, Xu H, Yun Y, Guo J, Chuang Y D, Huang H, Meng D, Wang J, Fu Z, Peng R, Knize R J, Brown G J, Zhai X and Lu Y 2016 *J. Appl. Phys.* **120** 084101

[26] Guedes E B, Abbate M, Ishigami K, Fujimori A, Yoshimatsu K, Kumigashira H, Oshima M, Vicentin F C, Fonseca P T and Mossanek R J O 2012 *Phys. Rev. B* **86** 235127

[27] Kapilashrami M, Zhang Y, Liu Y S, Hagfeldt A and Guo J 2014 *Chem. Rev.* **114** 9662

[28] Zheng L, Zhu X Q, Sui Y X, Xue J Z, Liu B and Pei M X 2015 *Chin. Phys. B* **24** 056101